Journal of Power Sources 273 (2015) 380–388

Contents lists available at ScienceDirect

Journal of Power Sources

journal homepage: www.elsevier.com/locate/jpowsour

Preparation, characterisation and optimisation of lithium battery anodes consisting of silicon synthesised using Laser assisted Chemical Vapour Pyrolysis

Ziga Veliscek [a, b], Lidija Slemenik Perse [a], Robert Dominko [a], Erik Kelder [b], Miran Gaberscek [a, *]

[a] National Institute of Chemistry, P.O. Box 660, SI-1001 Ljubljana, Slovenia
[b] Faculty of Applied Sciences, Delft University of Technology, Delft 2628-BL, The Netherlands

HIGHLIGHTS

- Laser assisted Chemical Vapour Pyrolysis was used for synthesis of silicon.
- The particle size can be tuned from 10 to 80 nm with narrow size distribution.
- The portion of oxidised sample is much smaller than with other methods.
- The small size requires significant changes in electrode preparation.
- Spraying was found as a very good alternative to casting.

ARTICLE INFO

Article history:
Received 9 June 2014
Received in revised form
7 September 2014
Accepted 16 September 2014
Available online 28 September 2014

Keywords:
Silicon
Anode
Lithium batteries
Laser assisted Chemical Vapour Pyrolysis
Rheology
particle size

ABSTRACT

Suitability of silicon prepared using Laser assisted Chemical Vapour Pyrolysis (LaCVP) as a potential anode material in lithium batteries is systematically investigated. Its compositional, morphological, physical-chemical and electrochemical properties are compared to a current benchmark commercial silicon. Important differences in particle size and particle composition are found which, as shown, affect critically the rheological properties of the corresponding electrode slurries. In order to overcome the rheological problems of prepared nanosilicon, we introduce and optimise a spraying method instead of using the usual casting technique for slurry application. Interestingly, the optimised electrodes show similar electrochemical performance, regardless of the particle size or composition of nanosilicon. This unexpected result is explained by the unusually high resistance of electrochemical wiring in silicon-based electrodes (about 60 Ohm per 1 mg cm^{-2} of active material loading). Despite that, the optimised material still shows a capacity up to 1200 mA h g^{-1} at a relatively high loading of 1.6 mg cm^{-2} and after 20 cycles. On the other hand, by decreasing the loading to below ca. 0.9 mg cm^{-2} the wiring problems are effectively overcome and capacities close to theoretical values can be obtained.

1. Introduction

Despite their great progress during past two decades, the Li-ion batteries are still in the phase of development and many parameters need to be further optimised. Concerning the energy density, there is still much room for improving both the positive and negative electrode materials [1]. Among the possible negative electrode materials (anodes), carbonaceous materials with a theoretical capacity of merely 372 mA h g^{-1} are still dominating the practical usage. Li alloys have long been considered as the most appropriate class of anode materials to replace the carbons. For example, the silicon-based anode has a much higher theoretical capacity (4200 mA h g^{-1} for $Li_{22}Si_5$, or 3600 mA h g^{-1} for $Li_{15}Si_5$) [2–5] than graphite, with silicon being cheap, abundant and non-toxic. In addition, silicon is a widely used material, so all the relevant processing technologies have already been well developed [6,7].

However, Si-based electrodes still have several issues that need to be resolved before eventual commercialisation. The biggest

* Corresponding author. Tel.: +386 1 4760 320; fax: +386 1 4760 300.
E-mail address: miran.gaberscek@ki.si (M. Gaberscek).

http://dx.doi.org/10.1016/j.jpowsour.2014.09.111
0378-7753/

Table 1
Varied experimental parameters of LaCVP reactor.

	D1	D2	D3
SiH_4 flow [l min^{-1}]	0.24	1.2	0.48
N_2 dilution flow [l min^{-1}]	2.16	1.2	1.92
Powder colour	Dark brown	Ochre	Green ochre[a]
Production rate [g h^{-1}]	16	81	33
Particle size [nm]	20	20.80[b]	50

[a] The colour is between colours of D1 and D2.
[b] Bimodal distribution.

Table 2
Specific surface and composition of samples.

	BET [m^2 g^{-1}]	Total Si [wt. %]	Elemental Si [wt. %]	SiO_2 [wt. %]
D1	114	91	83	17
D2	46	93	87	13
D3	76	98	96	4
A1	30	66	36	64

problem is the relatively poor cycling performance, usually associated with the big volume changes (up to 300%) upon lithium uptake and release during each charge/discharge cycle. The mechanical stresses resulting from the huge volume changes result in decrepitation of Si grains, cracking and delamination of the electrode material which, in turn, leads to loss of electric contact between the active particles and the current collector and, finally, to loss of capacity [8]. Several approaches to alleviate this problem have already been proposed [5,9,10]. While it is possible to prepare special structures (e.g. thin films [11], nanowires [12]) with excellent cycling performance and high capacity (per active material) the processing is very expensive and the amount of active material in these structures is too small for commercial application.

Here we check systematically if the problem of silicon cycling can be solved by introducing morphologically and chemically more homogeneous silicon compared to state-of-the-art commercial silicon. Following this goal, the synthesis of silicon was carried out using Laser assisted Chemical Vapour Pyrolysis (LaCVP) [13], a method by which the particle size and particle size distribution of silicon can be easily controlled. Additionally, LaCVP gives much purer silicon particles - containing less oxide. Comparing the LaCVP-derived and commercial silicon, we show that the critical step remains the preparation and deposition of electrode slurry onto metallic substrate. We show that appropriate modification of the conventional casting method or introduction of a rarely used method [14] – spraying – can lead to considerably easier and more controllable electrode preparation with an option of a straightforward upscaling. Finally, we demonstrate, explain and comment on the highly important effect of electrochemical wiring on the performance of silicon electrodes.

2. Experimental

2.1. Silicon nanoparticles synthesis

Silicon nanoparticles were produced by LaCVP from silane gas (SiH_4) in an oxygen free reactor. In this method a CO_2 laser intersects a flow of diluted silane gas. The laser initiates and maintains a thermal decomposition of silane according to the overall equation:

$$SiH_4(g) \xrightarrow{nh\nu} Si(s) + 2H_2(g) \quad (1)$$

The product is a very pure silicon powder, which is collected on a filter. Although the reactor atmosphere is oxygen free by design, the produced nanoparticles are covered with a thin layer of silicon oxide (silica). We believe this oxygen comes from impurities in the feed gases and from minute leakages of the whole system. Due to this silica layer the silicon nanoparticles are not pyrophoric and can be safely handled in air atmosphere.

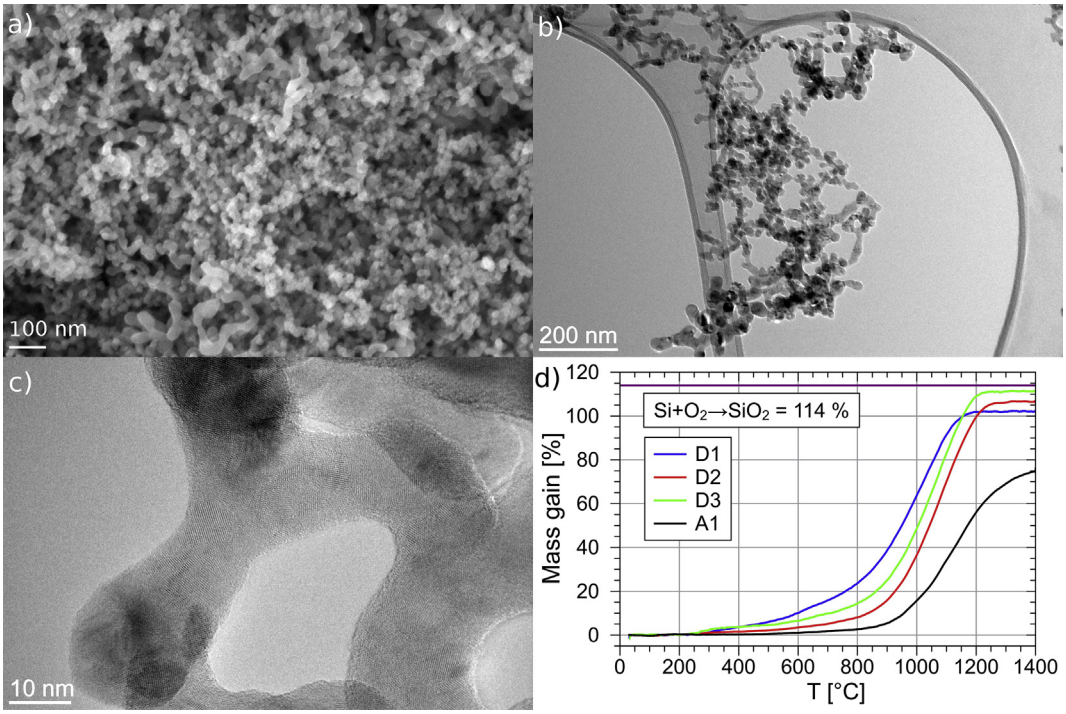

Fig. 1. Morphology of D1 as observed using different types of electron microscopy: a) SEM, b) TEM c) HR-TEM. d) TG analysis of samples prepared using LaCVP (D1, D2, D3) and commercial sample (A1).

A detailed description of LaCVP reactor used can be found elsewhere [13]. Three different batches are being discussed here, namely D1, D2, and D3. The reactor parameters that were constant between these batches are: reactor pressure, laser power, outer nozzle nitrogen flow, window flushing nitrogen flow and were respectively; 500 W, 800 mbar, 11.34 L min^{-1}, 20 L min^{-1}. Silane flow rate was varied from very small for batch D1 to maximum possible flow rate for batch D2. The D3 batch flow rate was set at twice the flow rate of D1. Dilution nitrogen flow was adjusted so that the linear velocity of diluted gas was 2.5 m s^{-1} for all batches. This way the residence time of silane in reaction region was identical. See Table 1 for numerical values and colours of produced powders (Table 2).

2.2. Electrode preparation

2.2.1. Preparation of anodes by casting

A casting slurry was prepared by mixing 160 mg of silicon nanoparticles (either self-synthesized using LaCVP or provided by Aldrich – Silicon nanopowder, <100 nm particle size –designated A1) and 24 mg of Carbon black (CB) (SuperP, MMM) in 2 mL of ethanol in a 10 mL beaker. The mixture was sonicated using a Hielcher probe sonicator UP200S for 2 min. A carboxymethylcellulose (CMC) (MTI) solution with a concentration of 10 mg mL^{-1} was prepared by dissolving an appropriate amount of CMC in a potassium citrate buffer with pH 3 using KOH (Aldrich) and citric acid (Aldrich). The CMC solution was left stirring overnight in order to thoroughly dissolve the CMC, and then stored in a fridge at 5 °C. Measured 1.6 mL of the so prepared CMC solution was added to a beaker and further sonicated for 5 min. The final volume of the slurry was 3.6 mL. The obtained slurry was tape cast on a Cu foil and dried in a vacuum drier at 90 °C at 300 mbar for 5 min. Circular electrode disks ($\Phi = 18$ mm) were punched out from the electrode coatings, dried overnight in a vacuum dryer and transferred to a glovebox.

2.2.2. Preparation of anodes by spraying

A spraying slurry was prepared using the same procedure as the casting slurry with the following differences: the volume of ethanol was 3 mL, the volume of the beaker was 25 mL, and an additional 6.4 mL of 30% ethanol was added after the CMC solution, giving a final volume of the slurry of 10 mL. The slurry was sprayed using a Fimotool DG-83 airbrush on a preweighed copper disc ($\Phi = 18$ mm) heated to 120 °C on a hot plate.

2.3. Rheology

The rheological measurements were performed with a rotational controlled rate rheometer (Physica MCR301, Anton Paar), equipped with a cone and plate sensor system (CP 50/2°). Oscillatory stress sweep tests at constant frequency of oscillation (1 Hz) were used in order to determine the linear viscoelastic range (LVR). Frequency tests were performed at constant small deformation in LVR by decreasing the frequency from 20 to 0.01 Hz. 3 step time tests were performed at three different steps, governing three steps to which the slurry is subjected: storage in the container, deposition on the substrate and the formation of dry coating. In the 1st and the 3rd step the slurry is subjected to the conditions with no shear. Therefore, these two steps were performed at constant small deformation in LVR, while in the 2nd step – during the application – the slurry is subjected to high shear. Hence, a high deformation was applied in this step. All rheological measurements were performed at constant temperature $T = 23$ °C.

2.4. Electrochemical testing

Galvanostatic discharge/charge measurements were carried out using two-electrode polymer-coated aluminium pouch cells with lithium metal as a counter electrode, and polypropylene/polyethylene separator (Celgard 2300). LP 40 (Merck) with 2% VC was used as electrolyte. The electrochemical testing was done on a Maccor 4200 galvanostat/potentiostat. In a typical cycling programme the potential was limited between 0.9 V and 50 mV unless noted otherwise and the current was C/50 in the first cycle and C/10 for all following cycles. The C-rate was based on the mass of the active material where the value of 4200 mA h g^{-1} was used as the theoretical capacity of Si (1C = 4200 mA). C-rates were calculated from the nominal electrode composition: Si:CB:CMC = 80:12:8 (wt. %). In a later stage, this was adjusted taking the residue of the buffer into account, giving the final weight ratio 69:10:7:14 for Si, CB, CMC, and buffer residue respectively.

In the case of spraying, the mass of deposited material can be easily determined as the copper disc can be weighed before and after deposition. However in the case of casting, it is very difficult to accurately determine the mass of the deposited material due to the inhomogeneity in the thickness of the copper foil. To determine the masses of the cast electrodes more accurately, the cells were disassembled after cycling, the active material was washed away and the copper discs were weighed. These masses then were used for the evaluation of the results.

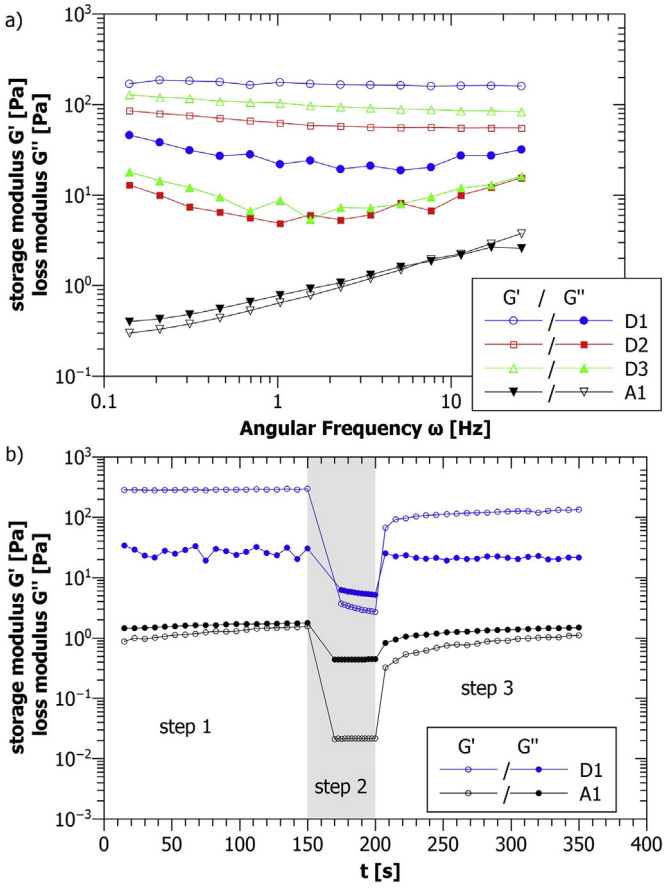

Fig. 2. a) Oscillatory frequency tests at constant deformation in LVR for LaCVP and commercial sample, b) 3-step tests for D1 and sample.

2.5. Characterization

Thermogravimetric (TG) measurements were performed on a Netzsch 409 C/CD instrument under a 100 mL min^{-1} flow of synthetic air (Ar:O_2 = 80:20) in a temperature range from 30 to 1400 °C, with a heating rate of 10 K min^{-1}.

Scanning Electron Microscopy (SEM), Cs probe corrected Scanning Transmission Electron Microscopy (STEM) and Focused Ion Beam (FIB) analysis was done on a Carl Zeiss Supra 35 VP, a JEOL ARM 200CF and an FEI Helios Nanolab650, respectively.

Brunauer–Emmett–Teller (BET) measurements were done on a Micromeritics ASAP 2020 device.

3. Results and discussion

3.1. Basic morphology of LaCVP-derived nanopowders

Using Laser assisted Chemical Vapour Pyrolysis (LaCVP) we prepared three batches of nanosized silicon, referred to as samples D1, D2, and D3. We tuned the silane flow rate with the aim to get different particle sizes in the range between approximately 20 and 100 nm. Morphological analysis using three kinds of microscopy showed that samples D1 (shown as example in Fig. 1) and D3 have monodisperse, more or less spherical, crystalline particles with average diameter approximately 20 nm and 50 nm, respectively. D2 sample has a bimodal size distribution with average diameters approximately 20 nm and 80 nm. All other morphological features of the three samples are similar. Although the spherical particles are not agglomerated, the structures contain joints, thereby forming “worm like” structures as shown in Fig. 1c. Fig. 1a–c reveals three important features of nanosilicon prepared using LaCVP (on the example of sample D1): it consists of well separated (non-agglomerated) particles, the particle size is quite uniform and on the surface of particles there is a thin amorphous layer of silica. Contrary to the commercial sample which contains up to 64 wt. % of silica, all of the LaCVP-derived samples are much purer and contain only a few % of silica, as revealed by TG analysis (Fig. 1d and Table 1). It is probably these differences that lead to different rheological properties, as discussed in continuation.

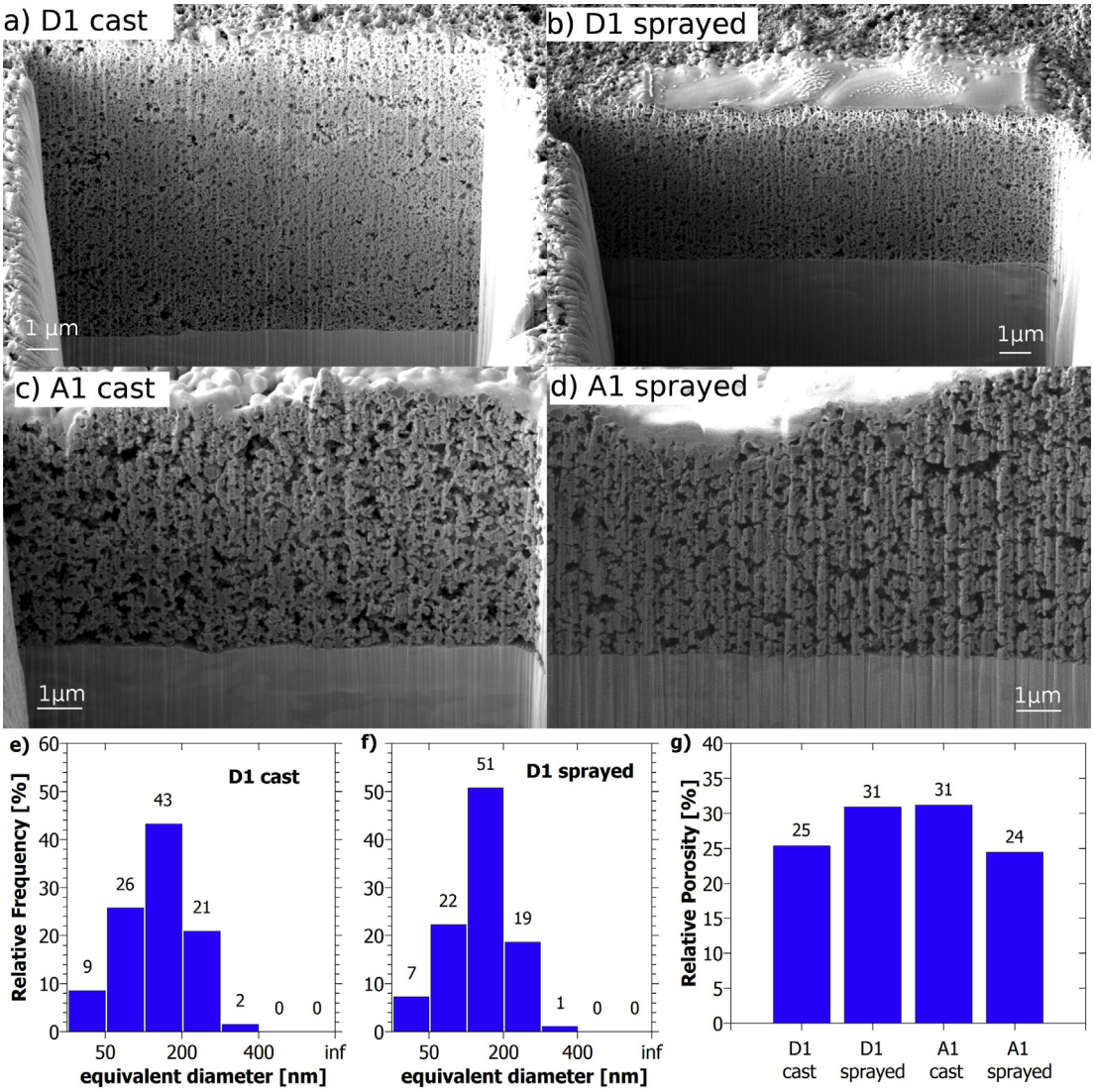

Fig. 3. Electrode cross-sections prepared using FIB. a) D1-cast, b) D1-sprayed c) A1-cast d) A1-sprayed. e, f) pore size distribution estimated using image analysis for D1-cast and D1 sprayed; g) mean pore size for cast and sprayed D1 and A1 determined from FIB image at a magnification of 20 k. While the difference in particle morphology of samples D1 and A1 can be observed, there is no apparent difference in porosity using casting and spraying method.

3.2. Optimisation of slurry preparation

We hypothesised that the considerable differences in morphology and chemical composition of LaCVP with respect to the more conventional (commercial) materials could importantly affect their electrochemistry when used as anode for Li batteries. In fact, the potential appropriateness of LaCVP silicon as anode material has already been demonstrated in a recent feasibility study [15]. In our work significant differences from conventional materials were observed already during preparation of slurries. For example, using the recipes described in previous references [16,17], the slurry based on LaCVP samples did not adhere sufficiently to the copper substrate. Upon drying, the slurry shrinks causing tensions in the composite material which lead to cracking, bending and in a severe case to delamination of the material, even before electrochemical testing. This behaviour was more pronounced in the case of electrodes with heavier loading. To circumvent this problem Munao et al. [15,18] used an Electrospray Deposition (ESD) technique to prepare thin film electrodes with LaCVP Silicon. In order to improve the electrode preparation procedure with a goal of achieving more compact and possibly thicker electrodes, we modified a range of parameters and even tried different alternative deposition methods. To get a quantitative insight into properties of various slurries, rheological tests were carried out.

Using this approach an optimized procedure for preparation of the slurry has been singled out. The procedure is described in detail in the Experimental section. The essential novelty is that we add all components of the slurry to one vessel (beaker) and homogenize it using a probe sonicator *in situ*. In this way, the transfer of material between vessels, and associated material and solvent losses, are eliminated. It was determined that the amount of solvent in the slurry plays a crucial role for good adhesion of the composite material to the current collector. A more viscous slurry gives better results in casting, however, a small amount of solvent leads to a less homogenous slurry. Using predissolved CMC, the amount of solvent needed was significantly reduced and a probe sonicator facilitated good homogenization, even in this small amount of solvent. In the case of spraying, the amount of solvent used can be much greater as solvent evaporates during deposition. A favourable side effect of using a single vessel for the slurry preparation is a more accurate determination of final slurry stoichiometry as errors associated with material loss are thus eliminated. The novel/optimised procedure is especially suited for the LaCVP-derived samples as shown in rheological tests in Fig. 2.

In the oscillatory frequency tests at constant deformation in linear viscoelastic range (LVO) (Fig. 2a), one can observe a poor frequency dependence of the dynamic moduli G' and G'' for samples D1–D3. Furthermore, G' has typical values above 10 Pa and G' is consistently higher than G'' for any given sample Di. This behaviour indicates a gel-like, stable dispersion and implies a long-term storage stability for these samples [19]. Conversely, the reference commercial sample A1 shows a frequency dependence of the dynamic moduli. Also, G' is slightly higher than G'' which indicates a weak gel behaviour, while increasing of dynamic moduli with increasing frequency of oscillation implies a tendency towards sedimentation.

The 3-step time test (Fig. 2b) shows that during storage (step 1) sample D1 exhibits a high stability against sedimentation ($G' > G''$) so no sagging is expected. During step 2 G'' is larger than G' which means the sample is in good condition for uniform application. Finally, during the formation of the final coating (step 3) $G' > G''$, moreover, the recovery of the moduli to initial values is slow; therefore good levelling and the formation of high quality thicker coatings could be expected.

In contrast to all D samples, for sample A1 the 3-step test shows that $G'' > G'$ during all steps, which reveals a tendency towards sagging and thereby finally a nonhomogeneous coating with low probability to achieving good quality thicker coatings. This means that while the novel procedure for slurry preparation is quite appropriate for LaCVP-derived nanosized silicon, the same recipe might not be suitable for use with other silicon samples. Most likely, slurry preparation should be optimized individually for each silicon type.

3.3. Deposition of slurry onto copper substrate

As shown later on, the electrochemistry of the silicon anodes prepared from the optimised slurry showed quite good results for both types of samples (LaCVP-derived and commercial). However, very high capacities could only be obtained with very thin electrodes having a loading smaller than about 0.5 mg of active mass per 1 cm^2 of geometric surface area of the copper current collector. We have tried to identify the reason for the worse performance at higher loading. Two types of problems were observed: (i) the adhesion of electrode mass to current collector was not optimal in thicker electrodes – this could lead to sudden failure; (ii) the capacity was consistently smaller at higher loadings even if the adhesion to electrode seemed to be good. In order to address the first problem (poor, irreproducible adhesion), we replaced the

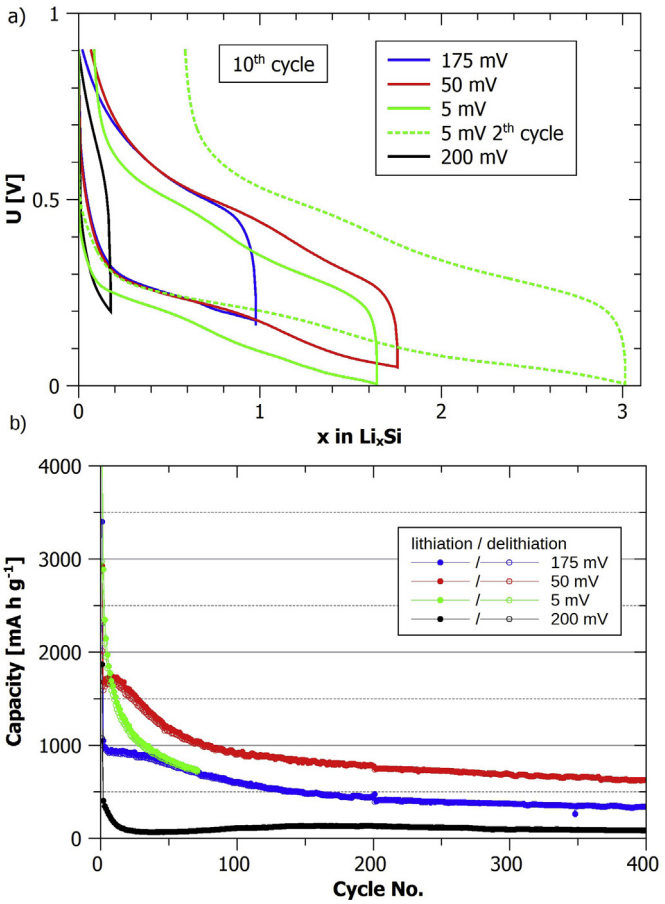

Fig. 4. The effect of lower-potential cut-off voltage on cycling behaviour (cast sample D1), a) charge/discharge curves of 10th and 2nd (dotted green curve) cycle to different cut-off voltages, b) specific capacities. Current rate: C/50 for 1st cycle, C/10 rest. (For interpretation of the references to colour in this figure legend, the reader is referred to the web version of this article.)

usual casting method [3,16,17] with a spraying method using an airbrush, as described in the Experimental section.

Indeed, the spraying method enabled much better adhesion of thicker electrodes. Furthermore, this method allows more precise loading and more homogeneous macroscopic features of deposit, giving a more uniform coating thickness. Most importantly, the porosity of the deposited film remains sufficient and homogeneous through the whole thickness, as demonstrated in FIB-cut cross sections displayed in Fig. 3.

Even if the spraying method removed the problem of poor adhesion, the other problem with thicker electrodes, i.e. the significant capacity drop, remained more or less unaffected: as soon as the loading approached to or exceeded ca. 1 mg cm^{-2}, the capacity started to drop significantly. We discuss this issue in considerable detail in the next section.

3.4. Electrochemical testing

In the literature the electrochemical testing of silicon has proceeded using surprisingly different protocols, see for example references [3,17,20,21]. As with other materials, one of the basic dilemmas is the selection of most appropriate electrochemical window. In the case of silicon very different values for the lower potential limit have been proposed, from 200 mV to 5 mV. The variable low-potential limit probably stems from the early paper by Obrovac and Krause [3], who assumed that for good reversible cycling a special core–shell structure (with crystalline core and amorphous shell) must be formed in the 1st cycle. Subsequent cycles were supposed to be carried out so that only the amorphous shell is used for storage of Li. The protocol proposed by Obrovac [3] (1st cycle to 50 mV and subsequent to 175 mV) was used on the sample D1 prepared by casting and the result is displayed in Fig. 4 (blue curve). Setting a lower cut-off voltage for all cycles (50 mV – red curve) one obtains a higher capacity while the cycling performance remains the same. Hence, the capacity degrades at the same rate as with higher cut-off. Setting the voltage even lower (5 mV) does not lead to further improvements and could be problematic due to possibility of plating of metallic lithium [22]. In contrast, cycling down to higher cut off voltages (100 mV 1st cycle, 200 mV subsequent cycles, Fig. 4a, black curve) decreases the capacity significantly. Based on these experiments we decided to use 50 mV as the standard low-potential cut off voltage. To validate this voltage a range of HR TEM analyses (Fig. 5) was performed on a fresh and cycled electrode. This particular sample with a loading of 0.32 mg cm^{-2} retained a capacity of 1132 mA h g^{-1} after 300 cycles. From Fig. 5 it can be seen that pristine silicon was crystalline (Fig. 5a, c) while the cycled electrode does not contain a crystalline silicon core (Fig. 5b, d). Therefore, we conclude, that a crystalline core is not necessary in the case of nanometric particles.

Setting up the most appropriate cycling protocol, we could directly compare the LaCVP-derived samples with the commercial sample using both deposition techniques - casting and spraying. Typical results collected from more than 50 different experiments are summarised in Fig. 6. The first conclusion from such a comparison is that at low enough loadings (about 0.5 mg cm^{-2}), the deposition method does not influence the electrochemistry regardless of the particular sample (D1, A1 etc). This can be explained by FIB images (Fig. 3) where also no major difference can

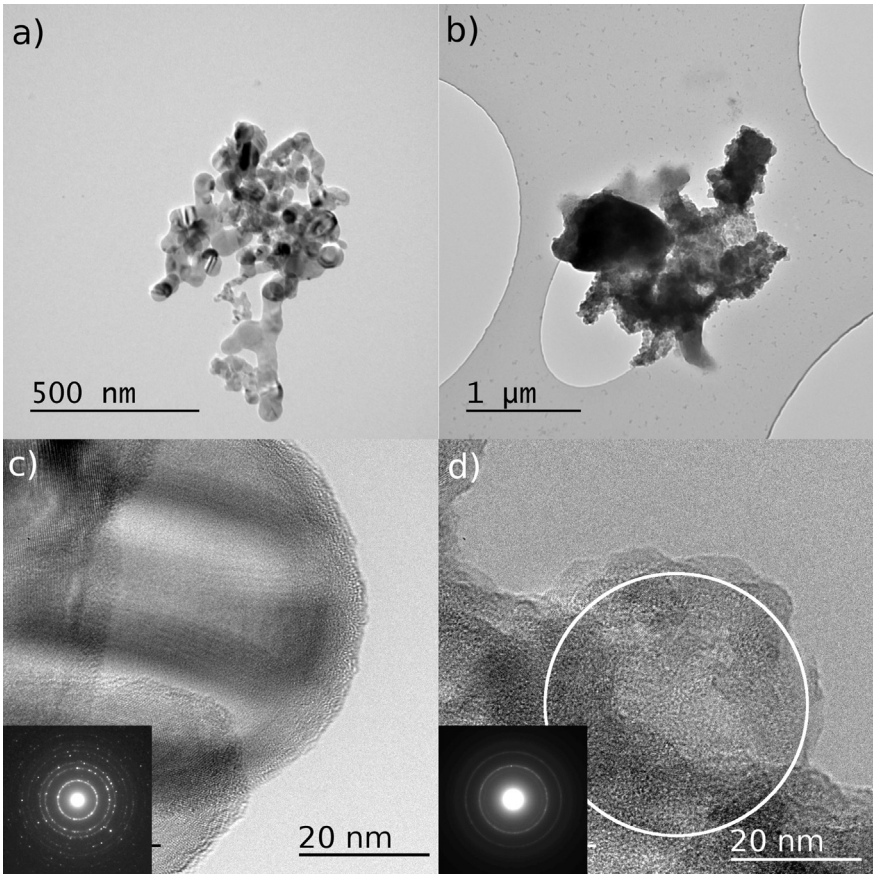

Fig. 5. HR TEM of a, c) fresh composite material and b, d) after 300 cycles. No crystalline silicon is observed after cycling. d) Originally spherical particles are highly deformed, circle outlines probable particle before cycling.

be observed between cast and sprayed samples. Similarly, increasing the loading (green curves), the capacity decreases. It is also interesting that both in sample D1 and sample A1, the capacity significantly increases after a certain number of cycles. However, whereas in sample D1, this happens between the 5th and 15th cycle, in sample A1, the capacity "hump" is observed only after about 100 cycles. The origin of this increase is unknown at the present state of research.

A broader overview of the electrochemistry of different samples (D1, D2, D3, A1) is shown in Fig. 7a. The effect of different loadings and the development during progressive cycling are displayed. As regards the capacity, the first cycles stand clearly out for all samples, consistently with previous studies [15,17,21]. The performance of commercial sample A1 is somewhat poorer, however, note that the slurry preparation was optimised for the nanosize LaVPC samples. In any case, probably the most consistent general message from Fig. 7a is that electrode loading determines crucially the performance of silicon electrodes. Particle size and other differences between D1, D2 and D3 seem less important. To get a clearer picture about this important behaviour, we first focus on a particular set of measurements, for example on the results of 10th cycle as shown in Fig. 7b. As indicated, we can roughly divide the points in Fig. 7b into two trends: up to about 0.9–1.0 mg cm^{-2} the capacity seems to be more or less constant, regardless of the batch of nanosilicon (D1, D2, D3). Above ca. 1.0 mg cm^{-2}, however, the capacity consistently decreases with increasing loading - in all three cases. In continuation we show that, very likely, the cause for this capacity drop is the increased electrode polarisation due to problems with electrochemical wiring at higher loadings.

The distinction between the electrochemical wiring and polarisation due to any process involving active particle (insertion, solid state diffusion, alloying, displacement reaction etc.) is schematically presented in Fig. 8a [23,24]. Electronic and ionic transport from current collector (or electrolyte) towards an active particle result in wiring resistances $R_{w,1,i}$ and $R_{w,2,i}$, respectively. Both resistances can be effectively summed up into $R_{w,i}$ (not shown). As the loading increases, the thickness of electrode also increases and so does the average length of electronic and ionic "wires". Thus, the total wiring resistance (for all particles), R_w, will be exactly proportional to the electrode loading (mass per area, m_A): $R_w \propto m_A$.

Very different scaling occurs in the case of resistance due to reaction/transport involving active particles, $R_{p,i}$. As the number of particle increases, the total surface area of all particles also increases which, however, leads to a decrease of the total particle-related resistance, R_p. More specifically, the total particle surface area increases exactly proportionally to the loading, which means that the total particle-related resistance R_p is exactly inversely proportional to the loading: $R_p \propto (m_A^{-1})$.

Thus, R_w and R_p behave exactly oppositely when the loading increases: the former increases while the latter decreases. This is the basis for the analysis shown in Fig. 8b. As demonstrated in our previous works, the total electrode resistance was extracted from

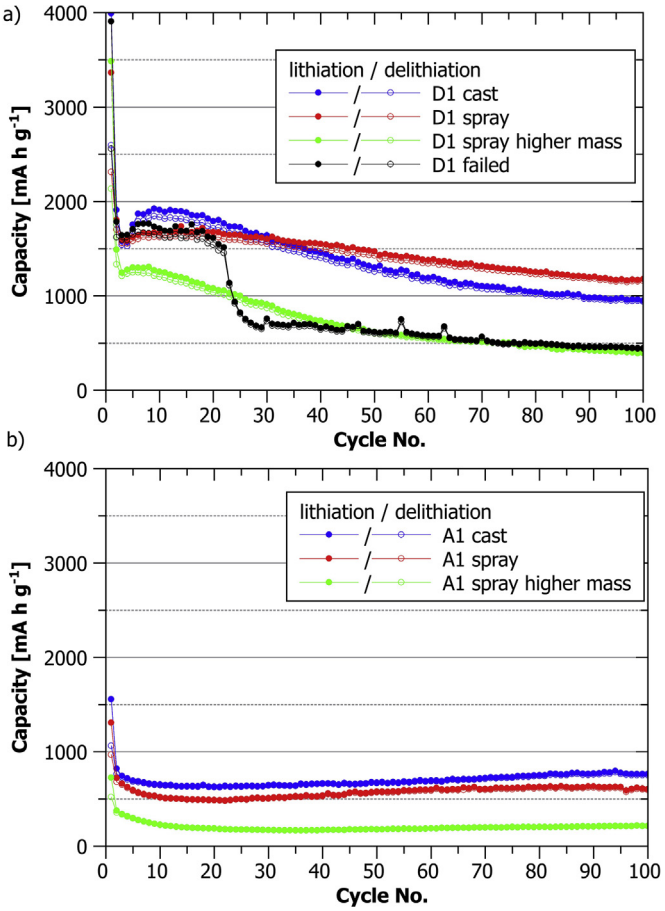

Fig. 6. a) Cycling of cast and sprayed electrodes based on D1. b) Cycling of cast and sprayed electrodes based on A1. Current rate: C/50 for 1st cycle, C/10 rest.

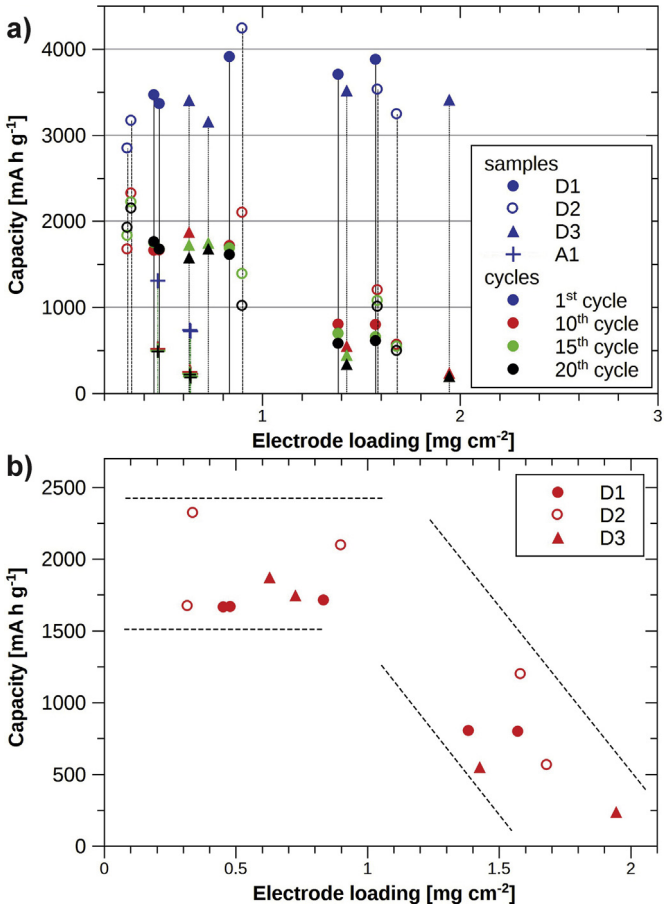

Fig. 7. a) Reversible capacity as a function of electrode loading for various samples tested in the present investigation. Current rate: C/50 for 1st cycle, C/10 rest. b) Enlarged view showing that the capacity-versus-loading behaviour can be roughly split into two parts – at low loadings the mass has negligible influence on capacity, at higher loadings the capacity starts to drop significantly.

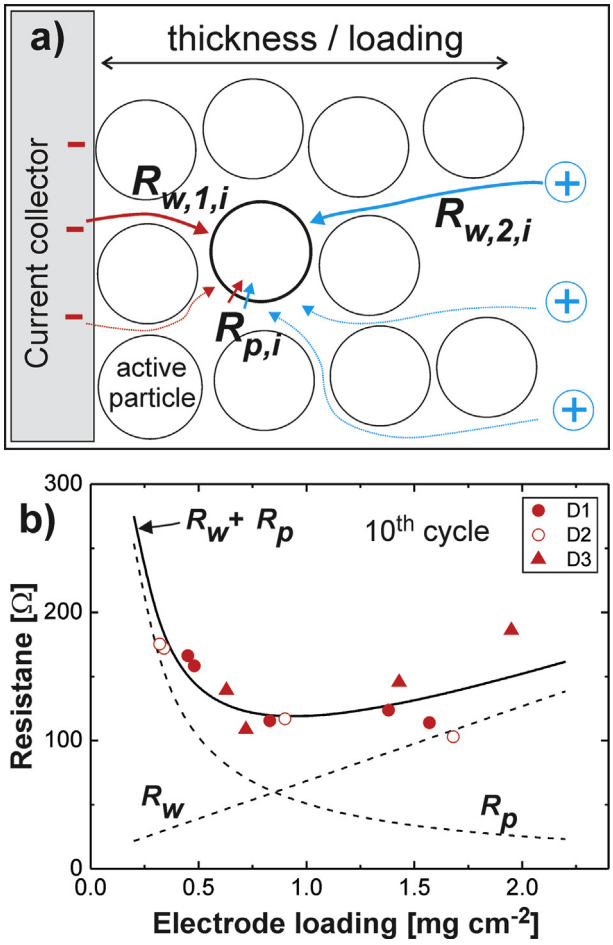

Fig. 8. a) Schematics showing that the overall transport in electrode can be split into two major contributions: the wiring (index "w") and the particle-related (index "p") processes. Both processes, in turn, can be split into ionic (blue arrows) and electronic (red arrows) contributions. More information is given in the main text. b) Measured (red symbols) and fitted (solid curve) dependence of electrode resistance as a function of electrode loading. The solid curve is split into individual (wiring, particle) contributions (dashed curves). (For interpretation of the references to colour in this figure legend, the reader is referred to the web version of this article.)

voltage polarisation at given state of charge ($x = 0.25$ was chosen in all cases) and dividing this polarisation with the current (note: the absolute currents rather than normalised currents, C-rates, need to be used to get the resistance in "ohms" displayed in Fig. 8b). We can see that the measured points display a minimum around 0.9–1.0 mg cm^{-2}. The points can be reasonably well fitted with the sum of theoretical *Rw* + *Rp* contributions (solid curve). It can be deduced that starting from the zero loading to the loading at the curve minimum the total resistance drops due to decreasing resistance of particle-related process, *Rp* – in this case the resistance due to alloying with Li. After that the resistance due to wiring, *Rw*, becomes the dominant contribution so the total resistance starts to increase. The transition from one to another type of dominating resistance (form *Rp* to *Rw*) coincides well with the transition from constant to dropping capacity in Fig. 7b. So, we might conclude that the capacity will remain unaffected until wiring problems, either due to electronic or ionic part, occur.

The significant contribution of wiring resistance already at small loading values (<1 mg cm^{-2}) certainly represents an important limitation for construction of silicon electrodes. For example, it is easy to deduce from Fig. 8b that if the wiring resistance was 6 times smaller, we would be able to construct electrodes with a loading >2.5 mg cm^{-2} which would exhibit a total resistance about 4 times smaller than in the present case – despite their much bigger thickness. The reason for the very high wiring resistance are unclear. We hypothesise that the main problem could be the poor electronic contact between the carbon black additive and the silicon nanoparticles. In any case the average wiring resistance per 1 mg of active material is about 60 Ω, which is about 15 times bigger than in the case of conventional $LiCoO_2$ cathode material [25].

Finally, let us point out clearly why the relatively high value of R_w (100 Ω mg at a loading of 1 mg cm^{-2}) crucially limits the electrode performance. Namely, such a value of resistance will cause an additional polarisation of about 42 mV at C/10. This additional polarisation shifts the whole discharge curve to lower potential values and causes a "premature" approach to cut off voltage and hence (much) lower capacities. Bearing this significant impact of wiring in mind, one could partly explain the variation of charge–discharge protocols, especially the low-potential limit, proposed by different authors, as discussed in the beginning of this subchapter. Namely, even relatively small variation in loadings or slurry preparation/deposition protocol could affect significantly the wiring resistance thus affecting the cut off voltage in an uncontrolled way.

4. Conclusions

Preparation of silicon using Laser assisted Chemical Vapour Pyrolysis (LaCVP) is fast (80 g h^{-1}) and allows some flexibility in tuning the particle size (10–80 nm) while the size distribution is relatively narrow. The portion of oxidised sample is very small (only several %). All these properties seem convenient for potential practical usages of the LaCVP derived nanosilicon.

However, the morphological and compositional differences to existing commercial silicon powders require significant changes in electrode preparation. Thus, slurries intended for casting of LaCVP silicon were prepared by adding all the components to one vessel and homogenizing it using a probe sonicator *in situ*. Fine adjustments of the amount of solvent in the slurry were needed to obtain a good adhesion of the composite material to the current collector. Using predissolved CMC, the amount of solvent needed was significantly reduced.

Spraying was found as a very good alternative to casting. Here the amount of solvent used could be much higher as solvent evaporates during deposition. Spraying effectively removed the problems of cracking even in the case of preparing thicker electrodes with LaCVP silicon.

Despite the careful optimisation of the slurry preparation and deposition methods, we observed that in thicker electrodes (loadings > ca. 1 mg cm^{-2}) the capacity dropped quite rapidly and consistently, regardless of the type of active material. Analysing the voltage polarisation using a simple quantitative model, we found that in silicon electrodes the contribution of electrochemical wiring resistance to the polarisation is surprisingly high (about 60 Ohms per 1 mg cm^{-2} of active material loading). One reason could be a poor electronic contacting between the active particles and carbon additives. If the wiring resistance could be reduced by a factor of 5–10, full utilisation of capacity could be obtained in electrode loadings as high as 2–4 mg cm^{-2}.

Acknowledgement

Financial support from the Slovenian Research Agency (National Programme No. P2-0148) is fully acknowledged. Additionally, Z. Veliscek acknowledges the support from Slovene Human Resources Development and Scholarship Fund (Ad Futura Scholarship). Part of the work was carried out within the FP7 project "Euroliion". We

thank G. Drazic, E. Tchernyshova, B. Novosel, and T. Skalar for FIB images, TEM images, TG and BET measurements, respectively. J.V. Erven and D. Munao are also gratefully acknowledged for their help with operating the LaCVP reactor.

References

[1] J.B. Goodenough, Y. Kim, Chem. Mater. 22 (2010) 587–603.
[2] M.N. Obrovac, L. Christensen, Electrochem. Solid State Lett. 7 (2004) A93–A96.
[3] M.N. Obrovac, L.J. Krause, J. Electrochem. Soc. 154 (2007) A103–A108.
[4] E. Radvanyi, E. De Vito, W. Porcher, J. Danet, P. Desbois, J.-F. Colin, S.J. Si Larbi, J. Mater. Chem. A 1 (2013) 4956–4965.
[5] U. Kasavajjula, C. Wang, A. Appleby, J. Power Sources 163 (2007) 1003–1039.
[6] D. Larcher, S.D. Beattie, M. Morcrette, K. Edström, J.-C. Jumas, J.-M. Tarascon, J. Mater. Chem. 17 (2007) 3759–3772.
[7] T.L. Kulova, Russ. J. Electrochem. 49 (2013) 1–25.
[8] J.H. Ryu, J.W. Kim, Y.-E. Sung, S.M. Oh, Electrochem. Solid State Lett. 7 (2004) A306–A309.
[9] W.-J. Zhang, J. Power Sources 196 (2011) 13–24.
[10] J.R. Szczech, S. Jin, Energy Environ. Sci. 4 (2011) 56–72.
[11] M. Uehara, J. Suzuki, K. Tamura, K. Sekine, T. Takamura, J. Power Sources 146 (2005) 441–444.
[12] C.K. Chan, H. Peng, G. Liu, K. McIlwrath, X.F. Zhang, R.A. Huggins, Y. Cui, Nat. Nanotechnol. 3 (2008) 31–35.
[13] J. van Erven, D. Munao, Z. Fu, T. Trzeciak, R. Janssen, E.M. Kelder, J.C.M. Marijnissen, KONA 27 (2009) 157–173.
[14] J. Guo, C. Wang, Chem. Commun. 46 (2010) 1428–1430.
[15] D. Munao, M. Valvo, J.W.M. van Erven, E.M. Kelder, J. Hassoun, S. Panero, J. Mater. Chem. 22 (2012) 1556–1561.
[16] D. Mazouzi, B. Lestriez, L. Roue, D. Guyomard, Electrochem. Solid State Lett. 12 (2009) A215–A218.
[17] S. Urbonaite, I. Baglien, D. Ensling, K. Edström, J. Power Sources 195 (2010) 5370–5373.
[18] D. Munao, J.W.M. van Erven, M. Valvo, E. Garcia-Tamayo, E.M. Kelder, J. Power Sources 196 (2011) 6695–6702.
[19] T. Mezger, The Rheology Handbook: for Users of Rotational and Oscillatory Rheometers, second ed., Vincentz Network, Hannover, 2006.
[20] D. Mazouzi, N. Delpuech, Y. Oumellal, M. Gauthier, M. Cerbelaud, J. Gaubicher, N. Dupré, P. Moreau, D. Guyomard, L. Roué, B. Lestriez, J. Power Sources 220 (2012) 180–184.
[21] J. Li, R.B. Lewis, J.R. Dahn, Electrochem. Solid State Lett. 10 (2007) A17–A20.
[22] V. Agubra, J. Fergus, Materials 6 (2013) 1310–1325.
[23] M. Gaberscek, M. Kuzma, J. Jamnik, Phys. Chem. Chem. Phys. 9 (2007) 1815–1820.
[24] M. Gaberscek, J. Power Sources 189 (2009) 22–27.
[25] M. Gaberscek, Acta Chim. Slov. 61 (2014) 480–487.